Conceptual and Numerical Model of Uranium(VI) Reductive Immobilization in Fractured Subsurface Sediments

ERIC E. RODEN[*,†] AND TIMOTHY D. SCHEIBE[*,‡]

Department of Biological Sciences, The University of Alabama, Box 870206, Tuscaloosa, AL 35487-0206, Pacific Northwest National Laboratory, P.O. Box 999, MS K9-36, Richland, WA 99352

* Address correspondence to either author. (E.E.R.) phone: (205) 348-0556; fax: (205) 348-1403; e-mail: eroden@bsc.as.ua.edu. (T.D.S) phone: (509) 372-6065; fax (509) 372-6089; e-mail: tim.scheibe@pnl.gov

† The University of Alabama

‡ Pacific Northwest National Laboratory

Abstract

A conceptual model and numerical simulations of bacterial U(VI) reduction in fractured subsurface sediments were developed to assess the potential feasibility of biomineralization at the fracture/matrix interface as a mechanism for immobilization of uranium in structured subsurface sediments. The model envisions flow of anaerobic groundwater, with or without acetate as an electron donor for stimulation of U(VI) reduction by dissimilatory metal-reducing bacteria (DMRB), within mobile macropores along a 1-dimensional flow path. As the groundwater moves along the flow path, U(VI) trapped in the immobile mesopore and micropore domains (the sediment matrix) becomes desorbed and transferred to the mobile macropores (fractures) via a first-order exchange mechanism. By allowing bacterial U(VI) reduction to occur in the mesopore domain (assumed to account for 12 % of total sediment pore volume) according to experimentally-determined kinetic parameters and an assumed DMRB abundance of 10^7 cells per cm^3 bulk sediment (equivalent to 4 mg of cells per dm^3 bulk sediment), the concentration of U(VI) in the macropore domain was reduced ca. 10-fold compared that predicted in the absence of mesopore DMRB activity after a 6-month simulation period. The results suggest that input of soluble electron donors over a period of years could lead to a major redistribution of subsurface uranium contamination in fractured subsurface sediments, converting potentially mobile sorbed U(VI) to an insoluble reduced phase (i.e. uraninite) in the mesopore domain that is expected to be permanently immobile under sustained anaerobic conditions.

Introduction

Uranium is an important radionuclide contaminant in soils and subsurface sediments at nuclear weapons manufacturing and uranium mining sites in the U.S. and abroad (*1*,*2*). The long half-life of ^{238}U (4.5×10^9 yr) and its decay to a suite of radioactive daughter products makes subsurface uranium contamination a significant environmental concern. For example, the risk posed by groundwater uranium contamination in the vicinity of uranium mill tailings exceeds that posed by high level nuclear waste subsequent to the decay of relatively short-lived (e.g., <600 years) isotopes (*1*).

Although aqueous U(VI) species are subject to surface complexation by particles in soils and sediments (*3*), in particular Fe(III) oxide surfaces (*3*-*9*), aqueous complexation of U(VI) by carbonate ions decreases the tendency of U(VI) to bind to mineral surfaces (*7*) and thereby enhances subsurface uranium migration. Since many subsurface environments contain substantial amounts of dissolved inorganic carbon (DIC), uranium can be relatively mobile in groundwater, and U(VI) is classified as a high mobility contaminant in the subsurface at several DOE sites (*10*). As a result, there is substantial interest in development of technologies for retarding uranium migration in subsurface sediments (*11*).

Uranium bioremediation via bacterial reductive immobilization. A promising approach for immobilization of uranium in the subsurface involves harnessing the activity of dissimilatory metal-reducing bacteria (DMRB) (*12*-*15*), which under anaerobic conditions catalyze enzymatic reduction of U(VI) to U(IV) via reactions such as:

$$2U(VI) + CH_2O \rightarrow 2U(IV) + CO_2 \qquad (1)$$

where CH_2O represents a generic unit of organic carbon. The significance of this reaction in terms of uranium mobility is that uranium in the +4 oxidation state tends to precipitate rapidly as

the insoluble mineral uraninite, $UO_2(s)$ (*16*). As a result, microbial uranium reduction can provide a mechanism for immobilization of uranium in subsurface environments via reactions such as:

$$2UO_2(CO_3)_2^{2-} + CH_2O + 2H_2O \rightarrow 2UO_2(s) + 5HCO_3^- + H^+ \qquad (2)$$

where $UO_2(CO_3)_2^{2-}$ represents the dominant aqueous U(VI)-carbonate complex in DIC-bearing solutions at circumneutral pH (*17*). A prerequisite for this process to operate effectively is the existence of anaerobic conditions in the aquifer sediments, because the DMRB are active only in the absence of O_2. Thus, unless a uranium-contaminated aquifer is *already* anaerobic, it would necessary to induce anaerobic conditions through addition of easily-degradable organic carbon, which would quickly deplete dissolved O_2 and render the system anaerobic. For the purpose of the conceptual development and numerical simulations presented in this paper, we assume that the subsurface environment is already anaerobic, and that DMRB have the potential to carry out U(VI) reduction when provided with suitable organic substrates.

An advantage of the above bioremediation strategy is that the DMRB that reduce and precipitate uranium can also utilize Fe(III) oxides as electron acceptors for anaerobic respiration (*15*). Many subsurface sediments contain substantial quantities of Fe(III) oxides. In such environments, addition of electron donors and nutrients would stimulate utilization of the large supply of endogenous electron acceptor provided by the Fe(III) oxides to generate and maintain DMRB biomass, which could then reduce and immobilize U(VI) moving through the treatment zone. This "in situ biogenic redox barrier" concept is analogous to processes involved in the formation of roll-front geological uranium ore deposits (*18*), in which U(VI) is reduced and precipitated along an advancing front localized at the interface between oxidized and reduced zones (*17*). Recent studies have demonstrated the feasibility of stimulating the growth and

activity of DMRB for Fe(III)/U(VI) reduction in previously well-oxidized subsurface sediments (*19-21*). The biogenic redox barrier concept may offer a far less costly and ultimately more effective approach to U(VI) remediation compared to protracted pump-and-treat operations for groundwater contaminant plumes which are dispersed over large areas and located 10's to 100's of meters below ground.

Potential complications in structured subsurface media. Although the U(VI) reductive immobilization strategy described above is conceptually sound, complications may arise during attempts to apply this approach to certain types of subsurface environments. Subsurface geologic materials often consist of a complex continuum of pore size domains ranging from macropores at mm and larger scales to micropores at μm to sub-μm scales. Fluid flow and solute transport rates in highly structured media (e.g. fractured subsurface sediments or soils with cracks or root macropores) can vary significantly among different pore domains. Structured media are characterized by high rates of advective flow and transport in large interconnected fractures, with diffusive mass transfer of solutes into and out of slowly-flowing or non-flowing pore zones (*22*). For example, saprolites at the Oak Ridge National Laboratory (ORNL), USA contain large fractures that carry the majority of groundwater flow but represent only a small fraction of the total porosity of the medium (*22-24*).

The physical structure of fractured subsurface media is likely to exert strong influence on coupled geochemical and microbial processes involved in contaminant bioremediation. Usually less than 20 % of total pore volume in structured media is accessible to bacteria (*25-27*), because most of the porosity is contained within micropores too small to accommodate the average bacterial cell (ca. 1-3 μm in diameter). This situation presents a major challenge for bioremediation because (i) bacteria are too large to effectively penetrate into the fraction of

sediment where the majority of contaminant mass typically resides, and (ii) the microporous matrix serves as a long-term source of contaminants that slowly diffuse into the faster flowing macropore domain. The latter phenomenon is particularly significant for contaminants that strongly interact with soil particles (e.g. uranium), because the micropore domain usually represents the dominant fraction of reactive surface area which serves as a repository for sorbed contaminant. Slow desorption of the contaminant in the micropore domain is thus likely to cause ongoing contaminant efflux into mobile fractures. A crucial unresolved issue in implementing bacterial U(VI) reduction for uranium bioremediation in fractured sediments (so far an untested technology at the field scale) is how to circumvent contaminant bleed-out from inaccessible micropores into the mobile macropore domain.

Uranium immobilization via biomineralization at the fracture-matrix interface – a hypothesis. Given the nature of fluid transport processes in fractured subsurface sediments, any solute that is hydraulically injected (e.g. a soluble electron donor to stimulate DMRB activity) will be preferentially transported into the macropore and (to a lesser extent) mesopore domains. While bacteria cannot physically access most of the micropore regime, they have the potential to grow in the meso- and macropore domains, and DMRB activity could therefore be stimulated by introduction of electron donors into those domains. Although these domains usually represent only a small fraction of the total porosity (see below), their spatial arrangements is such that stimulation of DMRB activity within them has the potential to produce biologically-reactive boundaries around the microporous matrix blocks where the bulk of radionuclide contamination resides (*22*,*28*). We hypothesize (see Fig. 1) that stimulation of DMRB growth and activity in these domains can lead to the formation of a localized, distributed semi-permeable redox microbarrier which retards mass transfer of U(VI) from the micropores to the more highly

conductive macropore domain. In this scenario, biomineralization – i.e. conversion of soluble U(VI) to insoluble $UO_2(s)$ – at the fracture/matrix interface would permit efficient immobilization of uranium contamination in sediments which would be difficult or impossible to remediate via other techniques.

Below we describe the results of numerical simulations designed to evaluate the above hypothesis, using information on the geological setting and hydrogeochemical conditions at the uranium-contaminated Area 2 site in the Bear Creek Valley at ORNL (*29*) as a basis for the simulations. We sought to assess the potential for bacterial U(VI) reduction at the fracture/matrix interface to reduce contaminant levels in mobile groundwater, which pose environmental risk through discharge to surface waters, or through movement into deeper aquifers and subsequent off-site transport (*22*). Because only limited site-specific information is available, several assumptions were required for this exercise. Accordingly, we recognize that the simulations are only illustrative of the hypothesized process and do not quantitatively predict performance at the field site. However, to the degree possible we underpinned our assumptions with field data and/or previous results, and the results provide strong qualitative support for the feasibility of the proposed U(VI) bioremediation strategy.

Model Design and Structure

Overview. The numerical simulations depict the flow of anaerobic groundwater, with or without acetate as an electron donor for stimulation of DMRB activity, along a 10-m, 1-dimensional subsurface flow path. As the groundwater moves along the flow path, U(VI) trapped in immobile mesopore and micropore domains is transferred via a first-order exchange mechanism to the mobile macropores (Fig. 2). In the presence of electron donor, DMRB growth and U(VI) reduction activity within the mesopore domain (see below) attenuates U(VI) mass transport into

the macropores, thereby inhibiting far-field uranium transport. The simulation includes 4 principal species (aqueous U(VI), sorbed U(VI), aqueous acetate, and solid-phase UO_2) in each of three pore size domains (see below) for a total of 12 primary dependent variables, which are listed in Table 1. The mass conservation equations for these variables are given in Appendix 1, and parameter values are listed in Table 2.

Pore domains and transport regimes. Gwo et al. (*24*) developed a multiple pore region (MPR) model of fluid/solute transport that successfully reproduced the results of nonreactive tracer transport experiments through saturated and unsaturated blocks of saprolite collected at ORNL (*23*). Based on their system conceptualization and quantitative model, we assume that the shale saprolites at ORNL are comprised of three distinct pore domains: macropores (> 500 μm diameter), mesopores (5–500 μm), and micropores (< 5μm). Pore volume contents of the three different domains, based on simulations of bromide transport conducted with the three-domain model MURT (*24*), are provided in Table 2.

Rates of advective fluid flow in the mesopore and micropore domains were assumed to be equal to zero. Hence, mass transport within these domains was limited to molecular diffusion. The rate of advective flow (Darcy velocity) in the macropore domain was set at 1 m d^{-1}, on the order of the groundwater flow rates at Area 2 (*29*). The exchange rate coefficients for mass transfer between the mobile and immobile domains were varied by trial-and-error in order to achieve (in the absence of bacterial U(VI) reduction activity) quasi-steady-state dissolved U(VI) concentrations (2-5 μM in the latter half of the 10-m spatial domain) comparable to average dissolved U(VI) concentrations measured in Area 2 groundwaters. The exchange rate coefficient for mass transfer between macropores and mesopores (ε_{12}; see mass conservation equations in Appendix 2) was set equal to that for transfer between the mesopore and micropore domains

(ε_{23}). The coefficient for transfer between macro and micropores (ε_{13}) was fixed at a value 10-fold lower than the other two coefficients in order to account for the longer diffusion path length between these two domains. In practice, the values of these coefficients are allowed to vary independently during fitting of data from nonreactive tracer transport experiments to a multiple-pore-region transport model (*24*). However, scaling issues prevent use of the best-fit exchange rate coefficients estimated for the laboratory core experiments analyzed in Gwo et al. (*24*) in simulations of field-scale solute transport, because the values of such coefficients depend strongly on the geometry of the three domains, and field-scale geometry is not fully represented in core-scale experiments.

U(VI) sorption/desorption. U(VI) sorption-desorption was assumed to follow a linear isotherm, and was modeled as a kinetic reaction with a relatively large rate constant (10 d^{-1}) such that near-equilibrium conditions were maintained. U(VI) sorption to the solid-phase within the flowing (macropore) domain was neglected, since the abundance of solid-surface per bulk volume of sediment in this domain is likely to be relatively low. The K_d value for U(VI) sorption (see Table 2) was derived from the results of diffuse double layer surface complexation modeling (based on the model described in Waite et al. (*7*); see Appendix 2 for details) in which the concentration of DIC was varied systematically in order to account for the influence of U(VI)-carbonate complexation on U(VI) adsorption. A DIC concentration of ca. 6 mM and constant pH of 6.5 (both based on typical values for Area 2 groundwaters at ORNL) were assumed in deriving the K_d value. Recent studies have demonstrated the ability of the Waite et al. model to accurately describe the sorption of U(VI) to natural subsurface materials (*30*).

U(VI) reduction by DMRB. For the purpose of these provisional simulations, we assumed that mesopore domain is the most likely place within structured subsurface media for

colonization and growth of DMRB capable of catalyzing U(VI) reduction (see Fig. 1). As discussed above, the micropores are too small to permit entry of bacteria with a characteristic size range of 1-3 μm. In addition, although the macropores may be sites for colonization (e.g. in the form of biofilms on fracture walls), relatively rapid rates of fluid flow and the absence of a large supply of solid-phase Fe(III) oxide as an electron acceptor for DMRB proliferation (due to the relatively low abundance of solid surface per volume of pore fluid in this domain) are likely to prevent major build-up of DMRB biomass. In contrast, experimental studies suggest that the surfaces of secondary fractures (assumed here to consist of a mixture of mesopores and micropores) are abundantly coated with Fe(III) and Mn(IV) oxides (*31*). These oxide phases are likely to provide a large source of electron-accepting capacity for growth and maintenance of DMRB populations within mesoscale pore regions accessible to μm-sized bacteria. Dissolved U(VI), a potentially important electron acceptor for DMRB growth and maintenance in uranium-contaminated subsurface media, is also likely to be present at relatively low concentrations in the macropores, due to rapid hydrological flushing. In contrast, mesopores are likely to possess substantially higher concentrations of U(VI) resulting from continual diffusion of U(VI) into the mesopores from the micropore domains.

Bacterial U(VI) reduction in the mesopore domain was modeled according to biomass-dependent dual Monod-kinetics (*32*) using V_{max} and K_m values (see Table 2) for U(VI) reduction determined for the acetate-oxidizing DMRB *Geobacter sulfurreducens* (see Fig. 3). The DMRB biomass used in the simulations is discussed in detail below. The U(VI) reduction kinetics experiments were conducted with washed acetate/fumarate grown *G. sulfurreducens* cells (ca. 10^8 mL^{-1}, equivalent to ca. 40 mg dry wt biomass L^{-1}) under non-growth conditions in PIPES (10 mM piperazine-N, N'-bis {2-ethanesulfonic acid}, dipotassium salt) buffered (pH 6.8) artificial

groundwater (*33*) containing 10 mM $NaHCO_3$ and 10 mM acetate. Changes in aqueous U(VI) concentration were determined hourly over a 3-hr incubation period with a Kinetic Phosphorescence Analyzer (Chemchek Instruments, Richland, WA), and rates of U(VI) reduction were determined by linear regression analysis of the [U(VI)] time course data. V_{max} and K_m values were estimated from nonlinear regression analysis of a plot of U(VI) reduction rate vs. initial U(VI) concentration. The values so obtained (Fig. 3) were comparable to those reported for other DMRB (*34*,*35*)

To our knowledge, no kinetic information is available on the dependence of acetate-oxidizing DMRB activity on acetate concentration. Therefore, a K_m value of 100 μM was assumed for the dependence of U(VI) reduction rate on acetate concentration based on the kinetics of acetate uptake by the acetate-oxidizing sulfate-reducing bacterium *Desulfobacter postgatei* (*36*). Testing showed that with the concentration of electron donor (acetate) in the infiltrating fluid set equal to 10 mM, acetate concentration did not have a strong influence on rates of U(VI) reduction, i.e. acetate was present in excess and U(VI) reduction rates were primarily dependent on the concentration of aqueous U(VI).

Potential inhibitory effects of nitrate (*37*,*38*) and Mn(IV) oxide (*39*,*40*) on U(VI) reduction were ignored in the simulations in order to focus the assessment on the capacity for in situ bacterial U(VI) reduction to scavenge μM-levels of U(VI) under more-or-less optimal conditions in situ. Although the presence of reactive Fe(III) oxides such as ferrihydrite can potentially inhibit bacterial U(VI) reduction (*41*), recent studies with natural uranium-contaminated subsurface sediments (amended with acetate to stimulate DMRB activity) suggest that bacterial Fe(III) oxide reduction and U(VI) reduction are likely to occur in concert with one another (*21*,*42*,*43*). Hence, our implict assumption that DMRB populations, whose growth and

maintenance is likely to be supported primarily by Fe(III) oxide reduction, are capable of carrying-out U(VI) reduction is consistent with existing information on the interactions between Fe(III) and U(VI) reduction during subsurface uranium bioremediation

Initial and boundary conditions. The concentration of U(VI) in the inflowing groundwater was set equal to 0.01 ppm (0.04 μM) based on average measured groundwater U(VI) values in well TMW05 in the vicinity of the up-gradient edge of the former Bear Creek channel at Area 2 (*29*). The relatively low concentrations of U(VI) in the inflowing groundwater reflects the localization of contaminated soils in the vicinity of the former channel caused by historical discharges of contaminated water down the former stream course and subsequent infiltration; groundwaters up-gradient and down-gradient of the former channel have low concentrations of U(VI) relative to the subsurface media directly below the former channel. The initial abundance of sorbed U(VI) in the three pore domains in the contaminated zone was set equal to 10^{-3} mol kg^{-1} based on measured values of total solid-phase uranium content of Area 2 sediments (*29*). The initial concentration of acetate in the three pore domains was set equal to zero, and the concentration of acetate in the inflowing groundwater was assumed to be constant at 10 mM. The initial concentration of dissolved U(VI) in the three pore domains was set equal to that of the incoming groundwater (0.04 μM); this was an arbitrary choice, as dissolved U(VI) concentrations rose quickly during the simulations to quasi-steady-state conditions (see below) as a result of desorption and mass transfer between the different pore domains.

Numerical solution. The coupled, nonlinear transport-reaction equations (Appendix 1) were integrated via the numerical method of lines (*44,45*) using the stiff ODE solver VODE (*46*). Relative and absolute error tolerances were set at 10^{-3} (0.1 %) and 10^{-12} (1 pM), respectively. Dispersive/diffusive and advective transport were modeled via finite difference, using central

differences and a blend of backward (upwind) and central differences (*47*), respectively. Dirichlet (constant concentration) and Neumann (zero gradient) boundary conditions were assumed for solutes at the upper and lower ends of the 10-m spatial domain, which was discretized on an even grid with 0.1 m node spacing.

Simulation Results and Interpretation

In the absence of biological U(VI) reduction, concentrations of U(VI) in the three pore domains increased rapidly as a result of desorption from the solids in the mesopore and micropore domains, and mass transport from the latter two domains into the macropores (Fig. 4A,B). The baseline simulations showed virtually no decrease in the concentration of aqueous and sorbed U(VI) in the mobile or immobile domains during a 6-month simulation period. These results illustrate explicitly how substantial amounts of aqueous U(VI) can persist in the mobile domain of saturated uranium-contaminated ORNL sediments (*29*) despite high rates of fluid flux through the macrofractures: slow release of U(VI) via desorption from solids in the saprolite matrix leads to continual bleed-in of contaminant into the mobile phase (e.g. Jardine et al. (*48*)). They also illustrate the well-known problem that traditional pump-and-treat procedures, which remove fluid primarily from the macropore domain, are generally ineffective as a means of contaminant remediation in structured media such as that present at ORNL: ongoing mass transfer of contaminant out of the immobile domain will slowly reintroduce U(VI) to the mobile phase as it is removed via pumping, with the result that pump-and-treat operations would have to be carried out for a very long period of time in order to substantially diminish the total pool of subsurface contamination. These considerations emphasize the attractiveness of harnessing of DMRB metabolism to drive in situ immobilization of redox-sensitive metal/radionuclide contaminants such as U(VI).

In order to assess the potential impact of enzymatic U(VI) reduction on U(VI) reactive transport in the hypothetical fractured subsurface sediment, we varied the assumed biomass of active DMRB in the mesopore domain in an attempt to achieve a ca. 10-fold decrease in dissolved U(VI) concentration in the mobile domain by the end of a 6-month simulation period. The question to be tested in this exercise was whether such a decline could be achieved with an environmentally-realistic DMRB biomass. The results (Fig. 4C) showed that with a steady-state mesopore DMRB biomass of 10^7 cells mL^{-1} (equivalent to 4 mg of cells per dm^3 bulk sediment), a progressive decline (to below 1 μM) in mobile-phase aqueous U(VI) concentration at the far end of the 10-m spatial domain was achieved over the 6-month simulation period. In addition, there was a marked decline in the abundance of aqueous and sorbed U(VI) in the mesopore domain relative to the abiotic simulations (Fig. 4D). In other words, enzymatic U(VI) reduction in the mesopores led to a global draw down of U(VI) in the mesopore domain. These results suggest that sustained input of soluble electron donors over a period of years could lead to a major redistribution of subsurface uranium contamination, converting potentially mobile sorbed U(VI) to an insoluble reduced phase (i.e. UO_2) in the mesopore domain that is be expected to be permanently immobile under anaerobic conditions (*17*).

It is important to note that the quantity of UO_2(s) (molar volume = 25 mol cm^{-3}) which accumulated in the mesopore domain during the simulation represents less than 0.1 % of the total pore volume associated with the mesopores. Similarly, the DMRB biomass of ca. 4 mg per dm^3 bulk sediment used in the simulation represents a total cell biovolume of less than 10^{-4} dm^3 per dm^3 bulk sediment (assuming an average cell diameter and length of 1 μm and 3 μm, respectively) – more than three orders of magnitude less than total mesopore volume. These calculations indicate that pore space constraints are not likely to substantially impede

development and maintenance of DMRB biomass during in situ biostimulation. Although production of ca. 10^7 cells mL^{-1} of DMRB biomass is almost certainly not achievable with the μM levels of aqueous U(VI) available as an electron acceptor in the mesopore domain, it is reasonable to assume that DMRB would be able to utilize endogenous solid-phase Fe(III) oxides as a major source of electron-accepting capacity for cell growth and maintenance. Fe(III) oxide surface coatings are very abundant in the ORNL saprolite, with total Fe(III) contents on the order of 20 g kg^{-1} (*49*). At an average bulk sediment porosity of 0.55, this corresponds to ca. 0.4 mol Fe(III) per dm^3 bulk sediment. Even if only a few % of the total Fe(III) oxide content is available for microbial reduction (*50*), this would provide sufficient electron-accepting capacity to produce ca. 10^8 cells mL^{-1} in the mesopore domain, assuming an average DMRB cell yield of ca. 5×10^6 cells per μmol Fe(III) reduced (*33,51*). The results of the numerical simulations suggest that the U(VI) reduction capacity of these organisms would be capable of producing a detectable decline in aqueous U(VI) concentrations in Area 2 groundwaters during a 6-month in situ biostimulation experiment.

In summary, our analysis provides strong support for the idea that in situ biostimulation of bacterial U(VI) reduction could lead to detectable changes in the total abundance, spatial distribution, and redox speciation of uranium in fractured subsurface sediments at Area 2 at ORNL. The simulations also generate specific, experimentally-testable predictions with regard to both microscale distributions of uranium within the pore space structure of sediments that have undergone microbial reduction, as well as macroscale changes in the temporal and spatial distribution of aqueous U(VI) along a 1-D flow path during biostimulation. Experimental sediment column and in situ field-scale experiments are underway to evaluate the validity of these predictions.

Table 1. Primary dependent variables included in the MPR simulation of U(VI) reactive transport in fractured subsurface media.

Variable	Explanation	Initial Value
$U(VI)aq_1$	Aqueous U(VI) in macropores	0.0 mol dm^{-3}
$U(VI)aq_2$	Aqueous U(VI) in mesopores	0.0 mol dm^{-3}
$U(VI)aq_3$	Aqueous U(VI) in micropores	0.0 mol dm^{-3}
$U(VI)ads_1$	Sorbed U(VI) in macropores	0.0 mol kg^{-1}
$U(VI)ads_2$	Sorbed U(VI) in mesopores	0.001 mol kg^{-1}
$U(VI)ads_3$	Sorbed U(VI) in micropores	0.001 mol kg^{-1}
Ac_1	Aqueous acetate in macropores	0.0 mol dm^{-3}
Ac_2	Aqueous acetate in mesopores	0.0 mol dm^{-3}
Ac_3	Aqueous acetate in micropores	0.0 mol dm^{-3}
$UO2_1$	Solid-phase UO_2 in macropores	0.0 mol kg^{-1}
$UO2_2$	Solid-phase UO_2 in mesopores	0.0 mol kg^{-1}
$UO2_3$	Solid-phase UO_2 in micropores	0.0 mol kg^{-1}

Table 2. Parameter values used in the MPR simulation of U(VI) reductive immobilization in fractured subsurface media.

Parameter	Units[a]	Value
θ_1	dm^3 H_2O dm^{-3} bulk (macropores)	0.09
θ_2	dm^3 H_2O dm^{-3} bulk (mesopores)	0.12
θ_3	dm^3 H_2O dm^{-3} bulk (micropores)	0.34
θ_T	dm^3 H_2O dm^{-3} bulk	0.55
ψ_T	kg dry sed dm^{-3} bulk	$\rho_s(1-\theta_T)$
ρ_s	kg dry sed dm^3 dry sed	2.5
v_1	dm H_2O d^{-1}	10.0
v_2	dm H_2O d^{-1}	0.0
v_3	dm H_2O d^{-1}	0.0
D^* (dispersion)	dm^2 d^{-1}	0.1
$Dm_{U(VI)}$ (diffusion)	cm^2 s^{-1}	10^{-6}
Dm_{Ac} (diffusion)	cm^2 s^{-1}	10^{-5}
$D_{U(VI)1} = D^* + Dm_{U(VI)}\theta_1^2$		
$D_{U(VI)2} = Dm_{U(VI)}\theta_2^2$		
$D_{U(VI)3} = Dm_{U(VI)}\theta_3^2$		
$D_{Ac1} = D^* + Dm_{Ac}\theta_1^2$		
$D_{Ac2} = Dm_{Ac}\theta_2^2$		
$D_{Ac3} = Dm_{Ac}\theta_3^2$		
ε_{12}	d^{-1}	0.005
ε_{13}	d^{-1}	0.0005
ε_{23}	d^{-1}	0.005
$k_{U(VI)ads2}$	d^{-1}	10
$k_{U(VI)ads3}$	d^{-1}	10
$Kd_{U(VI)2}$	dm^3 kg^{-1}	10
$Kd_{U(VI)3}$	dm^3 kg^{-1}	10
$Vmax_{U(VI)}$	(mol l U(VI) dm^{-3} d^{-1}) (mol Acetate dm^{-3})$^{-1}$ (g Biomass dm^{-3})$^{-1}$	0.0438
$Km_{U(VI)}$	mol U(VI) dm^{-3}	0.000361
Km_{Ac}	mol Acetate dm^{-3}	0.0001
Biomass	g dm^{-3}	0-0.004

[a] dm = decimeter; d = day

Fig. 1. Schematic diagram illustrating the concept of a distributed redox microbarrier. Panel A is a photograph of a trench excavated in saprolite material (structured with multiple pore domains). Physical scale is indicated by the size of lumber in the photo; other panels are not to scale. Panel B shows an expanded view of a portion of the trench in which dipping bedding planes are visible. Panel C is based on a different photograph of a core drilled from fractured saprolitic materials and conceptually represents structure at the scale of the highlighted box in Panel B. For illustrative purposes, light-colored areas of the photo have been highlighted in white, conceptually representing macroporous regions of the photograph. Panel D shows an expanded view of a portion of Panel C, with additional details showing mesoporosity (micro-fractures) within one of the porous blocks in white. Panel E is a representation of Panel D following biostimulation; black regions represent the formation of biomass at the interface between pore domains (for simplicity; only mesoporosity in the central block is represented). Contamination in the dark grey regions of Panel E (microporous zones) is inhibited from transporting into hydraulically accessible pore space indicated in white (macroporous zones) by reductive precipitation at the biologically-active interfaces.

Fig. 2. Conceptual diagram of the operation of the numerical simulation model.

Fig. 3. Kinetics of U(VI) reduction coupled to acetate oxidation by *Geobacter sulfurreducens* under nongrowth conditions in PIPES-buffered artificial groundwater medium containing 10 mM $NaHCO_3$. U(VI) reduction rates were determined via linear regression analysis of [U(VI)] vs. time data (triplicate 10-mL tubes for each U(VI) concentration) over a 3-hr incubation period.

Error bars represent ± the standard error of the linear regression slope parameter. The solid line represents a nonlinear least-squares regression fit of the data to Monod kinetic function.

Fig. 4. Breakthrough curves for aqueous U(VI) (A,C) in the macro (domain 1), meso (domain 2), and micro (domain 3) pores predicted by the MPR simulation model under abiotic (A) conditions (no enzymatic U(VI) reduction) or biotic (C) conditions. Also shown are the corresponding concentrations of solid-phase (sorbed) U(VI) and $UO_2(s)$ (B,D) at the far end of the 10-m flow path during the simulation period.

Fig. 1

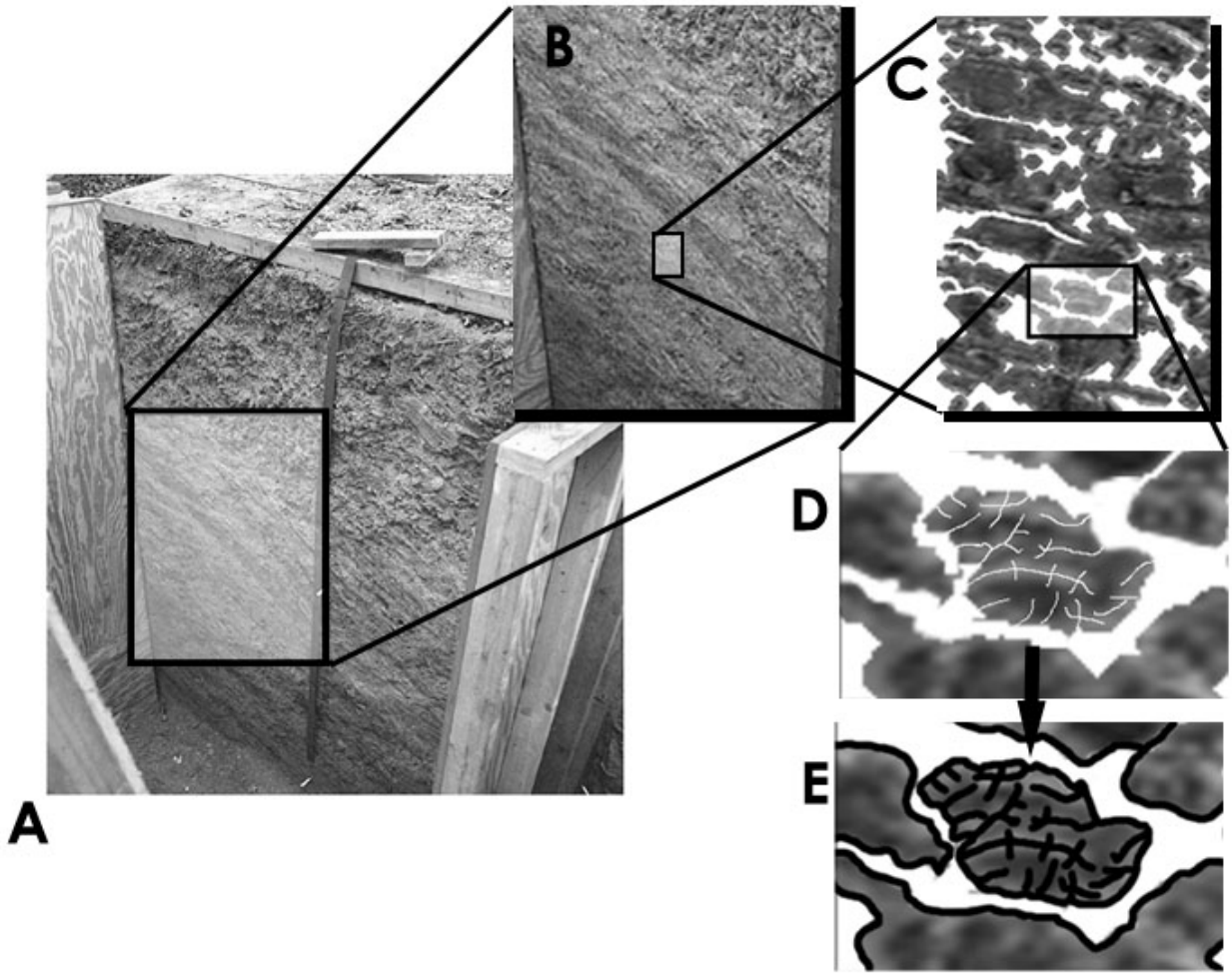

Fig. 2

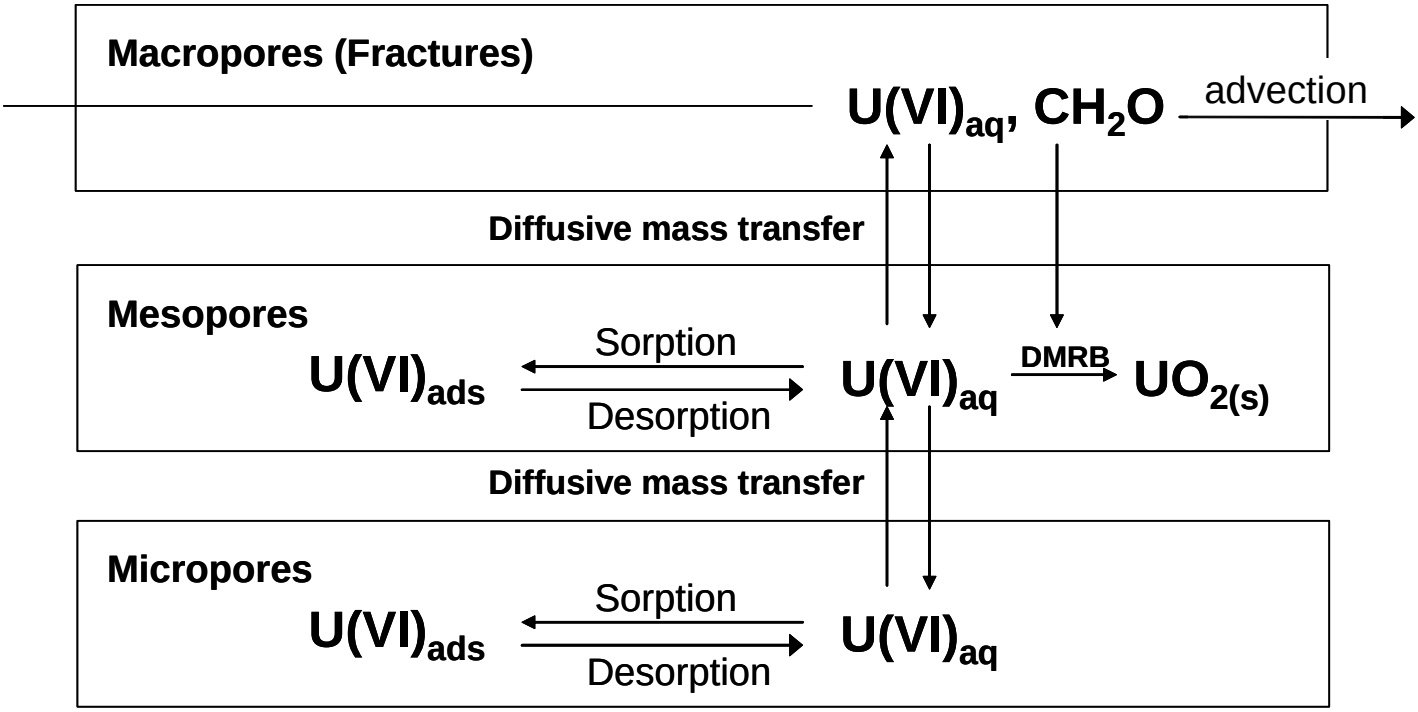
Macropores (Fractures)
U(VI)aq, CH2O
advection
Diffusive mass transfer
Mesopores
U(VI)ads
Sorption
Desorption
U(VI)aq
DMRB
UO2(s)
Diffusive mass transfer
Micropores
U(VI)ads
Sorption
Desorption
U(VI)aq

Fig. 3

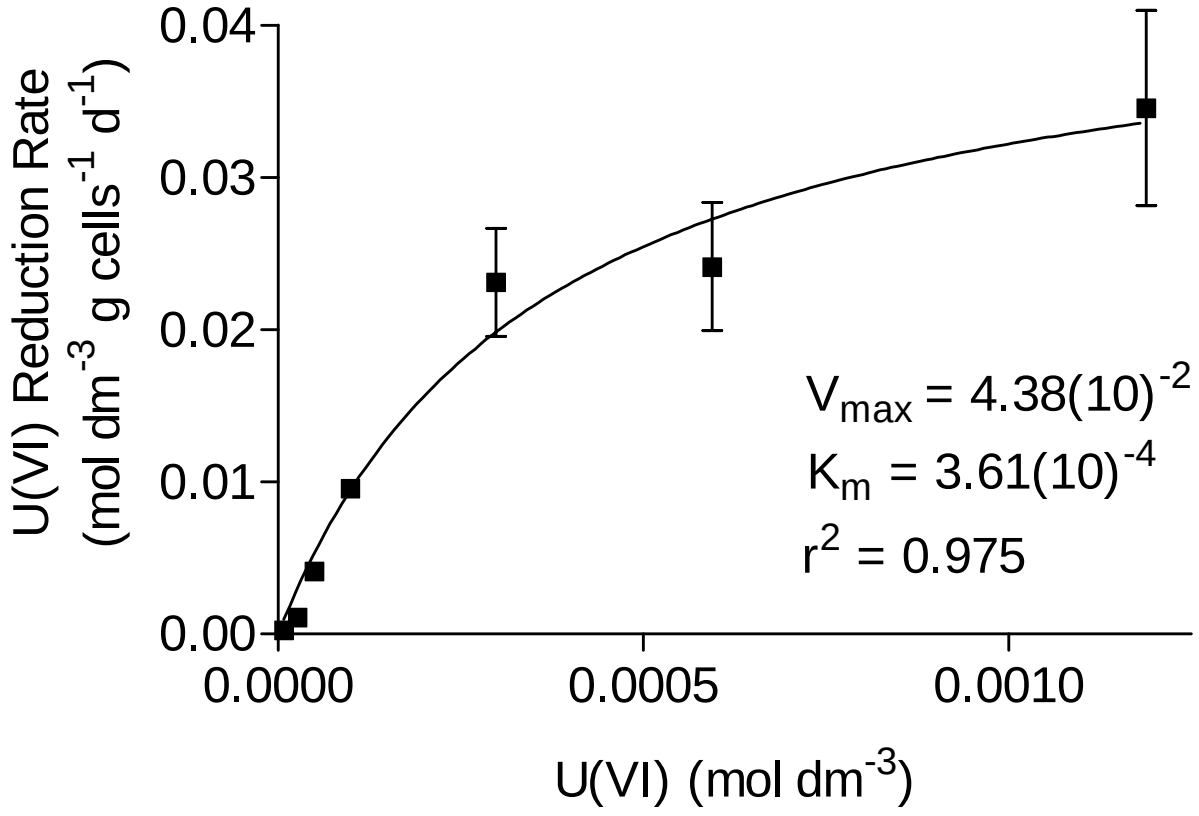
0.04
0.03
0.02
0.01
0.00
0.0000
0.0005
0.0010
U(VI) Reduction Rate
(mol dm-3 g cells-1 d-1)
U(VI) (mol dm-3)
Vmax = 4.38(10)-2
Km = 3.61(10)-4
r2 = 0.975

Fig. 4

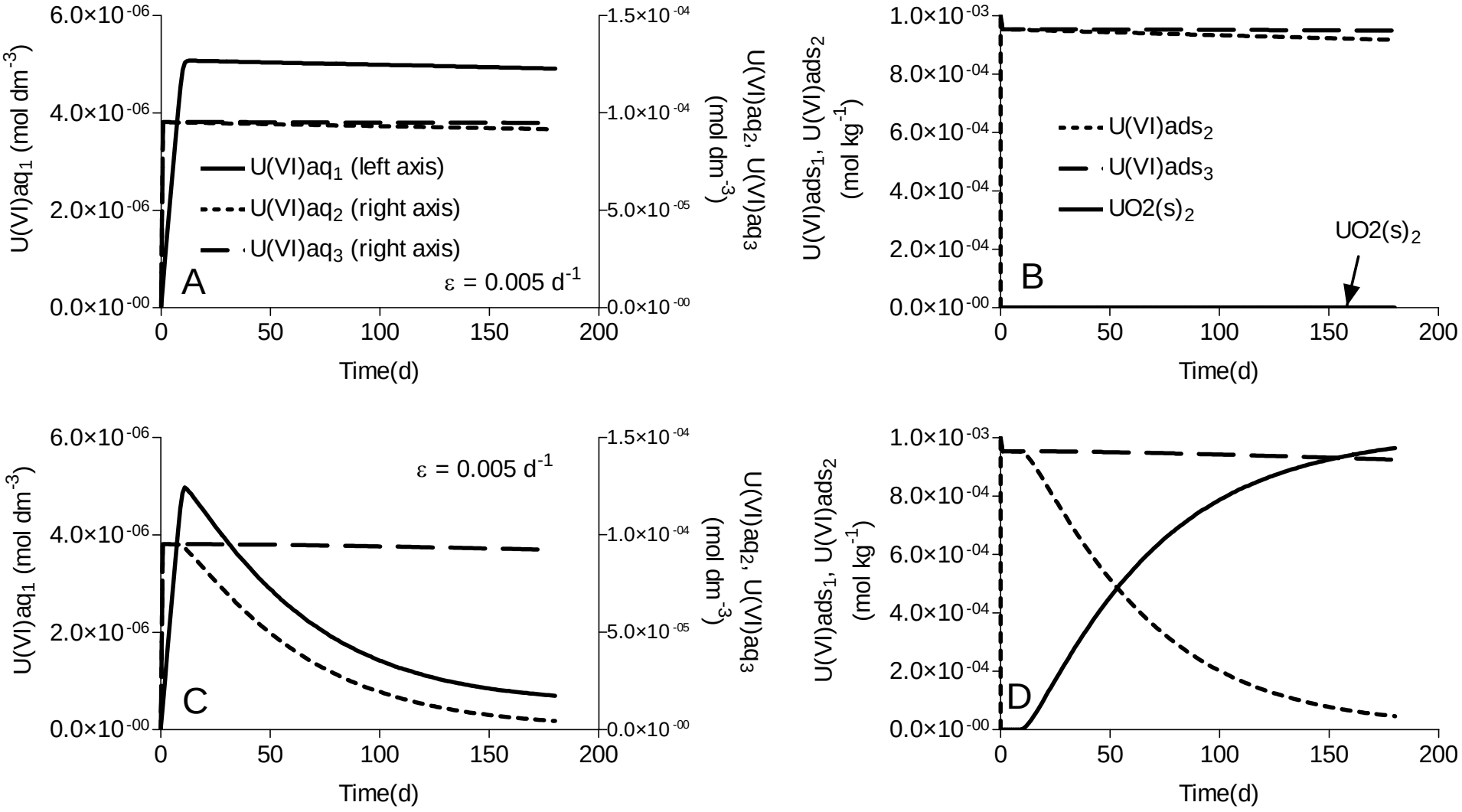
A
B
C
D
U(VI)aq1 (mol dm-3)
U(VI)aq2, U(VI)aq3 (mol dm-3)
U(VI)ads1, U(VI)ads2 (mol kg-1)
Time(d)
U(VI)aq1 (left axis)
U(VI)aq2 (right axis)
U(VI)aq3 (right axis)
ε = 0.005 d-1
U(VI)ads2
U(VI)ads3
UO2(s)2

Acknowledgements

This research was supported by funding from the U.S. Department of Energy, Natural and Accelerated Bioremediation Program. We thank Shawn Benner for review of an earlier version of the manuscript.

Literature Cited

(1) Landa, E. R.; Gray, J. R. *Environ. Geol.* **1995**, *26*, 19-31.

(2) Bradley, D. J.; Frank, C. W.; Mikerin, Y. *Phys. Today* **1996**, *49*, 40-45.

(3) Ticknor, K. V. *Radiochim. Acta* **1994**, *64*, 229-236.

(4) Hsi, C.-K. D.; Langmuir, D. *Geochim. Cosmochim. Acta* **1985**, *49*, 1931-1941.

(5) Kohler, M.; Wieland, E.; Leckie, J. O. In *Water-Rock Interaction*; Kharaka, Maest, Eds.; Balkema: Rotterdam, 1992; pp 51-54.

(6) Casas, I.; Casabona, D.; Duro, L.; Depablo, J. *Chem. Geol.* **1994**, *113*, 319-326.

(7) Waite, T. D.; Davis, J. A.; Payne, T. E.; Waychunas, G. A.; Xu, N. *Geochim. Cosmochim. Acta* **1994**, *58*, 5465-5478.

(8) Morrison, S. J.; Spangler, R. R.; Tripathi, V. S. *J. Contam. Hydrol.* **1995**, *17*, 333-346.

(9) Arnold, T.; Zorn, T.; Bernhard, G.; Nitsche, H. *Chem. Geol.* **1998**, *151*.

(10) DOE Subsurface Science Program: Program overview and research abstracts, U.S. Department of Energy, Office of Energy Research, Office of Health and Environmental Research,1991.

(11) NationalResearchCouncil *Research needs in subsurface science*; National Academy Press: Washington, DC, 2000.

(12) Lovley, D. R.; Phillips, E. J. P.; Gorby, Y. A.; Landa, E. R. *Nature* **1991**, *350*, 413-416.

(13) Gorby, Y. A.; Lovley, D. R. *Environ. Sci. Technol.* **1992**, *26*, 205-207.

(14) Lovley, D. R.; Phillips, E. J. P. *Environ. Sci. Technol.* **1992**, *26*, 2228-2234.

(15) Lovley, D. R. *Journal of Industrial Microbiology* **1995**, *14*, 85-93.

(16) Langmuir, D. *Geochim. Cosmochim. Acta* **1978**, *42*, 547-569.

(17) Langmuir, D. *Aqueous Environmental Geochemistry*; Prentice Hall: Upper Saddle River, NJ, 1997.

(18) Lovley, D. R.; Anderson, R. T. *J. Hydrol.* **2000**, *8*, 77-88.

(19) Abdelouas, A.; Lu, Y.; Lutze, W.; Nuttall, H. E. *J. Contam. Hydrol.* **1998**, *35*, 217-233.

(20) Snoeyenbos-West, O. L.; Nevin, K. P.; Anderson, R. T.; Lovley, D. R. *Microb. Ecol.* **2000**, *39*, 153-167.

(21) Holmes, D. E.; Finneran, K. T.; O'Neil, R. A.; Lovley, D. R. *Appl. Environ. Microbiol.* **2002**, *68*, 2300-2306.

(22) Jardine, P. M.; Sanford, W. E.; Gwo, J. P.; Reedy, O. C.; Hicks, S. D.; Riggs, J. S.; Bailey, W. B. *Water Resour. Res.* **1999**, *35*, 2015-2030.

(23) Jardine, P. M.; Jacobs, G. K.; Wilson, G. V. *Soil Sci. Soc. Am. J.* **1993**, *57*, 945-953.

(24) Gwo, J. P.; Jardine, P. M.; Wilson, G. V.; Yeh, G. T. *J. Hydrol.* **1995**, *164*, 217-237.

(25) Smith, M. S.; Thomas, G. W.; White, R. E.; Ritonga, D. *J. Environ. Qual.* **1985**, *14*, 87-91.

(26) Champ, D. R.; Schroeter, J. In *International Conference on Water and Waste Management*: Newport Beach, CA, 1988; Vol. 14, pp 1-7.

(27) McKay, L. D.; Cherry, J. A.; Bales, R. C.; Yahya, M. T.; Gerba., C. P. *Environ. Sci. Technol.* **1993**, *27*, 075-1079.

(28) Gwo, J. P.; O'Brien, R.; Jardine, P. M. *J. Hydrol.* **1998**, *208*, 204-222.

(29) Watson, D. B. *U.S. DOE, Natural and Accelerated Bioremediation (NABIR) Program, Field Research Center Web Site. http://www.esd.ornl.gov/nabirfrc/* **2002**.

(30) Barnett, M. O.; Jardine, P. M.; Brooks, S. C. *Environ. Sci. Technol.* **2002**, *36*, 937-942.

(31) Wilson, G. V.; Jardine, P. M.; O'Dell, J. D.; Collineau, M. *J. Hydrol.* **1993**, *145*, 83-109.

(32) Rittman, B. E.; VanBriesen, J. M. In *Reactive transport in porous media*; Lichtner, P. C., Steefel, C. I., Oelkers, E. H., Eds.; The Mineralogical Society of America: Washington, DC, 1996; Vol. 34, pp 311-334.

(33) Roden, E. E.; Urrutia, M. M.; Mann, C. J. *Appl. Environ. Microbiol.* **2000**, *66*, 1062-1065.

(34) Truex, M. J.; Peyton, B. M.; Valentine, N. B.; Gorby, Y. A. *Biotech. Bioengin.* **1997**, *55*, 490-496.

(35) Liu, C.; Gorby, Y. A.; Zachara, J. M.; Fredrickson, J. K.; Brown, C. F. *Biotechnol. Bioengin.* **2002**, *80*, 637-649.

(36) Ingvorsen, K.; Zehnder, A. J. B.; Jorgensen, B. B. *Appl. Environ. Microbiol.* **1984**, *47*, 403-408.

(37) Finneran, K. T.; Holmes, D. E.; Snoeyenbos-West, O. L.; Ciufo, S. A.; VanPraagh, V. G.; Long, P. E.; Lovley, D. R. In *American Society for Microbiology, 101st Annual Meeting, Abtract Q-33*, 2001.

(38) Senko, J. M.; Istok, J. D.; Suflita, J. M.; Krumholz, L. R. *Environ. Sci. Technol.* **2002**, *36*, 1491-1496.

(39) Fredrickson, J. K.; Zachara, J. M.; Kennedy, D. W.; Liu, C.; Duff, M. C.; Hunter, D. B.; Dohnalkova, A. *Geochim. Cosmochim. Acta* **2002**, *In press*.

(40) Liu, C.; Zachara, J. M.; Fredrickson, J. K.; Kennedy, D. W.; Dohnalkova, A. *Environ. Sci. Technol.* **2002**, *36*, 1452-1459.

(41) Wielinga, B.; Bostick, B.; Hansel, C. M.; Rosenzweig, R. F.; Fendorf, S. *Environ. Sci. Technol.* **2000**, *34*, 2190-2195.

(42) Finneran, K. T.; Anderson, R. T.; Nevin, K. P.; Lovley, D. R. *Soil Sed. Contamin.* **2002**, *11*, 339-357.

(43) Finneran, K. T.; Housewright, M. E.; Lovley, D. R. *Environ. Microbiol.* **2002**, *4*, 510-516.

(44) Schiesser, W. E. *The Numerical Method of Lines*; Academic Press: New York, 1991.

(45) Boudreau, B. P. *Diagenetic models and their implementation*; Springer: New York, 1997.

(46) Brown, P. N.; Byrne, G. D.; Hindmarsh, A. C. *SIAM J. Sci. Stat. Comput.* **1989**, *10*, 1038-1051.

(47) Fiadeiro, M. E.; Veronis, G. *Tellus* **1977**, *29*, 512-522.

(48) Jardine, P. M.; Fendorf, S. E.; Mayes, M. A.; Larsen, I. L.; Brooks, S. C.; Bailey, W. B. *Environ. Sci. Technol.* **1999**, *33*, 2939-2944.

(49) Barnett, M. O.; Jardine, P. M.; Brooks, S. C.; Selim, H. M. *Soil Sci. Soc. Am. J.* **2000**, *64*, 908-917.

(50) Roden, E. E.; Urrutia, M. M. *Geomicrobiol. J.* **2002**, *19*, 209-251.

(51) Roden, E. E.; Zachara, J. M. *Environ. Sci. Technol.* **1996**, *30*, 1618-1628.

Appendix 1. Mass conservation equations for model of U(VI) reductive immobilization in fractured subsurface media.

$$\theta_1 \frac{\partial U(VI)aq_1}{\partial t} = -v_1\theta_1 \frac{\partial U(VI)aq_1}{\partial x} + \theta_1 D_{U(VI)1} \frac{\partial^2 U(VI)aq_1}{\partial x^2} + \theta_1 R_{12_{U(VI)}} + \theta_1 R_{13_{U(VI)}} - \theta_1 R_{U(VI)ads1} - \theta_1 R_{U(VI)bio1}$$

$$\theta_2 \frac{\partial U(VI)aq_2}{\partial t} = -v_2\theta_2 \frac{\partial U(VI)aq_2}{\partial x} + D_{U(VI)2}\theta_2 \frac{\partial^2 U(VI)aq_2}{\partial x^2} - \theta_2 R_{12_{U(VI)}} + \theta_2 R_{23_{U(VI)}} - \theta_2 R_{U(VI)ads2} - \theta_2 R_{U(VI)bio2}$$

$$\theta_3 \frac{\partial U(VI)aq_3}{\partial t} = -v_3\theta_3 \frac{\partial U(VI)aq_3}{\partial x} + D_{U(VI)3}\theta_3 \frac{\partial^2 U(VI)aq_3}{\partial x^2} - \theta_3 R_{13_{U(VI)}} - \theta_3 R_{23_{U(VI)}} - \theta_3 R_{U(VI)ads3} - \theta_3 R_{U(VI)bio3}$$

$$\psi_T \frac{\partial U(VI)ads_1}{\partial t} = \theta_T R_{U(VI)ads1}$$

$$\psi_T \frac{\partial U(VI)ads_2}{\partial t} = \theta_T R_{U(VI)ads2}$$

$$\psi_T \frac{\partial U(VI)_3}{\partial t} = \theta_T R_{U(VI)ads3}$$

$$\theta_1 \frac{\partial \mathrm{Ac}_1}{\partial t} = -v_1\theta_1 \frac{\partial \mathrm{Ac}_1}{\partial x} + D_{\mathrm{Ac}1}\theta_1 \frac{\partial^2 \mathrm{Ac}_1}{\partial x^2} + \theta_1 R_{12_{\mathrm{Ac}}} + \theta_1 R_{13_{\mathrm{Ac}}} - \alpha_{U(VI)}\theta_1 R_{U(VI)bio1}$$

$$\theta_2 \frac{\partial \mathrm{Ac}_2}{\partial t} = -v_2\theta_2 \frac{\partial \mathrm{Ac}_2}{\partial x} + D_{\mathrm{Ac}2}\theta_2 \frac{\partial^2 \mathrm{Ac}_2}{\partial x^2} - \theta_2 R_{12_{\mathrm{Ac}}} + \theta_2 R_{23_{\mathrm{Ac}}} - \alpha_{U(VI)}\theta_2 R_{U(VI)bio2}$$

$$\theta_3 \frac{\partial \mathrm{Ac}_3}{\partial t} = -v_3\theta_3 \frac{\partial \mathrm{Ac}_3}{\partial x} + D_{\mathrm{Ac}3}\theta_3 \frac{\partial^2 \mathrm{Ac}_3}{\partial x^2} - \theta_3 R_{13_{\mathrm{Ac}}} - \theta_3 R_{23_{\mathrm{Ac}}} - \alpha_{U(VI)}\theta_3 R_{U(VI)bio3}$$

$$\psi_T \frac{\partial UO2_1}{\partial t} = \theta_T R_{U(VI)bio1}$$

$$\psi_T \frac{\partial UO2_2}{\partial t} = \theta_T R_{U(VI)bio2}$$

$$\psi_T \frac{\partial UO2_3}{\partial t} = \theta_T R_{U(VI)bio3}$$

where:

$$R_{12_{U(VI)}} = \varepsilon_{12}(U(VI)aq_2 - U(VI)aq_1)$$
$$R_{13_{U(VI)}} = \varepsilon_{13}(U(VI)aq_3 - U(VI)aq_1)$$
$$R_{23U(VI)} = \varepsilon_{23}(U(VI)aq_3 - U(VI)aq_2)$$

$$R_{12_{Ac}} = \varepsilon_{12}(Ac_2 - Ac_1)$$

$$R_{13_{Ac}} = \varepsilon_{13}(Ac_3 - Ac_1)$$

$$R_{23_{Ac}} = \varepsilon_{23}(Ac_3 - Ac_2)$$

$$R_{U(VI)ads1} = 0.0$$

$$R_{U(VI)ads2} = k_{U(VI)ads2}\left(U(VI)aq_2 - \frac{U(VI)ads_2}{Kd_{U(VI)2}}\right)$$

$$R_{U(VI)ads3} = k_{U(VI)ads3}\left(U(VI)aq_3 - \frac{U(VI)ads_3}{Kd_{U(VI)3}}\right)$$

$$R_{U(VI)bio1} = 0.0$$

$$R_{U(VI)bio2} = V\max_{U(VI)}\left(\frac{U(VI)aq_2}{Km_{U(VI)} + U(VI)aq_2}\right)\left(\frac{Ac_2}{Km_{Ac} + Ac_2}\right)\left(\frac{K_I}{K_I + NO3_2}\right)Biomass$$

$$R_{U(VI)bio3} = 0.0$$

Appendix 2. Estimation of K_d value for U(VI) sorption onto ORNL subsurface sediments.

Following the approach of Barnett et al. (2002), the Waite et al. (1994) parameters for U(VI) adsorption onto hydrous ferric oxide (HFO) were used to model U(VI) sorption onto a hypothetical Fe(III) oxide-containing sediment in order to develop an appropriate K_d value for simulating U(VI) adsorption-desorption in ORNL Area 2 sediments. This approach assumes implicitly that U(VI) sorption is dominated by interaction with Fe(III) oxide surfaces. This assumption is defensible as a first approximation in light of (i) the high abundance of Fe(III) oxide coatings on ORNL sediments (Barnett et al., 2000); and (ii) recent studies which indicated that U(VI) adsorption onto the rock material phyllite (composed of quartz, muscovite, chlorite, and albite) is dominated by interactions with small amounts of secondary ferrihydrite (Arnold et al., 1998; Schmeide et al., 2000), and that U(VI) adsorption onto Fe-rich kaolinitic natural materials could be well-predicted by assuming the presence of a single ferrihydrite-like component (Waite et al., 2000). The Waite et al. (1994) equilibrium constants for U(VI) adsorption, as well as those for aqueous U(VI)-hydroxyl and -carbonate species, were inserted into the diffuse layer model (DLM) of Dzombak and Morel (1990) and used develop isotherms for U(VI) sorption, assuming a range of total U(VI) concentrations of 10^{-7} to 10^{-3} M, and a range of total dissolved inorganic carbon (ΣDIC) concentrations of 10^{-4} to 10^{-2} M. A constant pH of 6.5 (based on typical values for Area 2 groundwaters at ORNL), ionic strength of 0.1M, and temperature of 25 °C were assumed for all calculations. The density of "strong" and "weak" Fe(III) oxide surface sites were computed using the DCB-extractable Fe content of the "Oak Ridge" subsurface materials studied by Barnett et al. (2000; 2002) (which had a DCB-extractable Fe content of 25.8 g kg^{-1}) and the site density (moles of strong and weak sites per mol of Fe) given in Dzombak and Morel (1990). A volumetric Fe(III) oxide concentration of 10 mmol Fe L^{-1} was assumed for all the calculations, which corresponds to a total solids concentration of 21.7 g L^{-1}.

The results (Fig. 1A) illustrate the strong influence which formation of aqueous U(VI)-carbonate complexes is likely to have on U(VI) adsorption onto Fe(III) oxide surfaces, with estimated K_d values decreasing exponentially with increasing ΣDIC (Fig. 1B). Groundwater ΣDIC values for Area 2 at ORNL range from 60-90 mg C L^{-1} (Watson,), which correspond to 5-7.5 mM. According to the curve-fit shown in Fig. A3.1B, these ΣDIC concentrations would result in K_d values for U(VI) sorption of 5.9-13.1. Based on these results, a K_d value of 10.0 was employed in the simulations of U(VI) reactive transport in ORNL sediments.

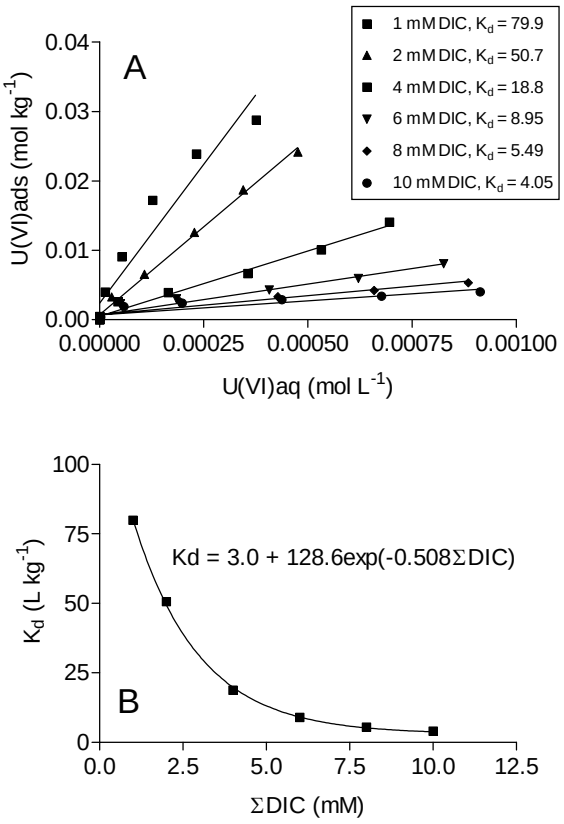

Figure 1. Calculation of K_d values for U(VI) sorption onto hypothetical FRC Area 2 sediments based on results of DLM simulations using the U(VI) HFO surface complexation and aqueous phase speciation parameters from Waite et al. (1994), and a range of assumed ΣDIC concentrations (all at pH 6.5, I = 0.1M, T = 25 °C) (Panel A), and relationship between estimated K_d for U(VI) adsorption and ΣDIC (Panel B).

References

Arnold, T., T. Zorn, G. Bernhard, and H. Nitsche. 1998. Sorption of uranium(VI) onto phyllite. Chem. Geol. 151.

Barnett, M.O., P.M. Jardine, and S.C. Brooks. 2002. U(VI) adsorption to heterogeneous subsurface media: application of a surface complexation model. Environ. Sci. Technol. 36:937-942.

Barnett, M.O., P.M. Jardine, S.C. Brooks, and H.M. Selim. 2000. Adsorption and transport of U(VI) in subsurface media. Soil Sci. Soc. Am. J. 64:1-43.

Dzombak, D.A., and F.M.M. Morel. 1990. Surface Complexation Modeling: Hydrous Ferric Oxide, John Wiley & Sons.

Schmeide, K., S. Pompe, M. Bubner, K.H. Heise, G. Bernhard, and H. Nitsche. 2000. Radiochim. Acta 88:723-728.

Waite, T.D., J.A. Davis, B.R. Fenton, and T.E. Payne. 2000. Radiochim. Acta 88.

Waite, T.D., J.A. Davis, T.E. Payne, G.A. Waychunas, and N. Xu. 1994. Uranium(VI) adsorption to ferrihydrite: Application of a surface complexation model. Geochim. Cosmochim. Acta 58:5465-5478.

Watson, D.B. (2002). U.S. DOE, Natural and Accelerated Bioremediation (NABIR) Program, Field Research Center Web Site. http://www.esd.ornl.gov/nabirfrc/